Kormányos et al. *NPG Asia Materials* (2025) 17:18
https://doi.org/10.1038/s41427-025-00598-4

NPG Asia Materials

ARTICLE Open Access

Application of Co_3O_4 as anode catalyst in CO_2 electrolyzer cells

Attila Kormányos[1], Tatiana Priamushko[2], Gergely F. Samu[3], Angelika Samu[1,5], Balázs Endrődi[1,4], Serhiy Cherevko[2] and Csaba Janáky[1,4,5]

Abstract

Replacing Ir with anode catalyst materials that are more abundant is a long-sought objective within the CO_2 electrolysis community. The chemical environment (near-neutral pH, carbonate buffer electrolyte) that inherently develops during long-term operation, however, limits the pool of applicable candidates. In this contribution, Ir was replaced with a porous Co_3O_4 nanosheet catalyst layer as the anode of a zero-gap CO_2 electrolyzer cell. The catalyst was directly deposited on the Ti porous transport layer via hydrothermal synthesis, which allowed the precise control of the catalyst loading. Under optimal conditions (7 mg cm^{-2} Co_3O_4 loading), 300 mA cm^{-2} current density was reached at 3.4 V applied cell voltage. The electrolyzer cell with the Co_3O_4 anode was operated continuously for 50 hours at 250 mA cm^{-2} current density with stable cell voltage and CO_2 reduction selectivity.

Introduction

Iridium is the most frequently employed anode catalyst in CO_2 electrolysis[1]. However, due to mainly economic reasons, and its instability under certain CO and CO_2 reduction conditions[2], its replacement with more abundant and stable catalysts has been a long-sought objective of the electrolysis community. While it seems to be a straightforward task at first glance, several peculiarities of CO_2 electrolysis must be considered, to find the right anode catalyst material. The anode and cathode compartments are typically separated by an anion exchange membrane (AEM), and in these cases, carbonate ions are the main species maintaining ion conduction (especially at high current densities)[3]. This means that during the operation of the electrolyzer cell, a high carbonate flux crosses over the membrane from the cathode to the anode side and directly hits the anode catalyst layer. If the anolyte is recirculated (which must be the case in any practical application), the continuous transport of carbonate ions gradually decreases the anolyte pH until a near-neutral value is reached (a carbonate/bicarbonate buffer solution forms)[3]. This is a key difference compared to AEM water electrolyzers, where the OH^- ions crossing over the AEM are immediately neutralized by the H^+ ions formed at the surface of the anode catalyst during water oxidation (OER)[4]. This is the reason why materials such as Ni, which shows high activity and stability in alkaline media, can only be used in CO_2 electrolysis if the anolyte pH is continuously monitored and adjusted by the addition of concentrated alkaline electrolyte to preserve its alkaline character[3].

Based on the above considerations, first and foremost, *the ideal catalyst candidate should show high OER activity in near-neutral pH electrolytes* containing carbonate/bicarbonate ions in high concentrations. Secondly, it should be composed of cheap and abundant materials (that are ideally not declared as critical raw materials) (https://single-market-economy.ec.europa.eu/sectors/raw-materials/areas-specific-interest/critical-raw-materials_en), and that can be synthesized by a method that is readily scalable to meet the needs of large-scale electrolyzer cells. Precedent reports on near-neutral OER were carried out mostly either in borate or phosphate buffer solutions[5]. In contrast, only a handful of research employed carbonate buffer solutions[1,6,7]. Catalysts in these studies are mostly based on Cu, Fe, Ni, Co, or even

Correspondence: Attila Kormányos (kormanyos.attila@szte.hu) or Csaba Janáky (janaky@chem.u-szeged.hu)
[1]Department of Physical Chemistry and Materials Science, University of Szeged, Rerrich Square 1, Szeged, Hungary
[2]Forschungszentrum Jülich GmbH, Helmholtz-Institute Erlangen-Nürnberg for Renewable Energy (IET-2), Cauerstraße 1, Erlangen, Germany
Full list of author information is available at the end of the article

Ir, and their common feature is that the active form develops during the OER[6–11]. The formation of transition metal carbonates can stabilize metals that are otherwise unstable at the near-neutral pH environment[3], such as Ni[12]. Such a catalyst-electrolyte interaction was observed first in the case of Co in a neutral pH electrolyte solution containing phosphate ions[13].

Research on Co-based oxides dates back to the 1980s'[14]. Since then, Co-based oxides gained most notable attention due to their high OER activity and durability in alkaline media[15,16]. The durability of Co_3O_4 in alkaline electrolytes lies in its low dissolution rates. However, a reversible structural and morphological alteration of the catalyst surface has been observed under OER conditions[17]. More closely, an amorphous $CoO_x(OH)_y$ layer with di-μ-oxo-bridged $Co^{4+/3+}$ ions forms on top of Co_3O_4. The development of these sites is an essential condition for Co_3O_4 to drive the OER[17]. The demonstration of the stability of Co_3O_4 in neutral phosphate anion-containing electrolytes[13], was followed by the application of Co_3O_4 in near-neutral and even acidic electrolytes[18–21]. Furthermore, Co_3O_4 has already been tested as an anode catalyst in pure water electrolysis[22,23] and in neutral pH seawater electrolysis[24]. In the former examples, the short-term (20 h) OER performance of Co_3O_4 matched closely with the values obtained for IrO_2 at $j = 500\ mA\ cm^{-2}$ applied current density. It was demonstrated that OER activity can be maintained even for 250 hours at the same current density, keeping the degradation rate below $1\ mV\ h^{-1}$. Similarly to IrO_2, the reason behind the observed degradation is mainly due to ionomer oxidation coupled with the change in surface composition/morphology. One of the main issues with Co_3O_4 is that it is intrinsically a semiconductor, which in turn results in higher cell voltage.

Co_3O_4 has a spinel structure[15], in which it is relatively easy to incorporate other cations (di-, and trivalent), which opens the possibility to tailor its intrinsic properties. There are many examples in the literature where the bare Co_3O_4 structure was doped with Pd, Cr, Fe, Ni, etc[15,24,25]. Besides cations, Co_3O_4 can be modified by other elements (e.g., F and N) too[26,27]. The purpose of the various dopants is to tailor the electronic structure of the catalyst, leading to improved charge transfer and, hence, higher OER activity and increased durability in acidic electrolytes (corrosion resistance of bare Co_3O_4 at acidic pH is moderate). The resulting modified Co_3O_4 anodes were successfully applied in polymer electrolyte membrane water electrolyzers, achieving high current densities (over $1\ A\ cm^{-2}$) at low overpotentials in acidic electrolytes approaching the performance of state-of-the-art noble metal systems (e.g., RuO_2)[25,26].

In contrast to water electrolysis[28], to our knowledge, no information is available on how Co_3O_4 behaves in the environment that develops during long-term CO_2 electrolysis with recirculated electrolyte (near-neutral pH carbonate buffer). According to thermodynamics, bare Co oxides are only stable at relatively high overpotentials in such an environment, in the potential regime where OER typically proceeds[12]. However, these statements have not been verified under CO_2 electrolysis conditions where kinetic effects could alter predictions from thermodynamics.

In this study, Ir was replaced with porous Co_3O_4 as the OER catalyst in a CO_2 electrolyzer cell. Co_3O_4 was prepared via a hydrothermal method allowing the direct deposition of the catalyst on the Ti porous transport layer (PTL). This approach resulted in direct contact between the catalyst and the PTL, which is critically important in achieving high-performance CO_2 electrolysis. The synthesis method is scalable; it is only limited by the size of the substrate and the autoclave. The electrochemical performance was probed in a zero-gap electrolyzer cell as a function of the thickness of the catalyst layer. The experienced stable long-term activity and CO2RR selectivity highlight the possible use of this alternative anode catalyst to replace scarce and expensive catalysts in CO_2 electrolyzer cells.

Materials and Methods

Chemicals

Cobalt nitrate hexahydrate ($Co(NO_3)_2 \cdot 6H_2O$, ≥98%, Sigma-Aldrich), urea ($CO(NH_2)_2$, 99.0-100.5%, Sigma-Aldrich), ammonium fluoride (NH_4F, ≥99.99%, Sigma-Aldrich), cesium hydroxide (Sigma-Aldrich), isopropanol (IPA, WVR), Ag nanoparticles ($d < 100$ nm, Sigma-Aldrich), Ir black ($d = 4$-6 nm, FuelCellStore), and commercial Co_3O_4 nanoparticles (NPs) (US Research Nanomaterials Inc., $d = 30$-50 nm) were purchased in analytical grade and used without further purification. The Nafion ionomer dispersion (10 wt%), Ti porous transport layer (PTL, 250 μm thickness) and the Freudenberg H23C6 carbon-based gas diffusion layer (GDL) was acquired from FuelCellStore. The PiperION anion exchange membrane (40 μm thickness), along with the PiperION ionomer (A5-HCO_3-EtOH) used in the cathode catalyst layer, was purchased from Versogen. All solutions were prepared using MilliQ grade (Millipore Direct Q3-UV, 18.2 MΩ cm) ultrapure water. A 4.5 purity CO_2, and 4.7 purity Ar were used to perform the electrolysis measurements. Both gases were purchased from Messer.

Preparation of the anode and cathode catalyst layers

Prior to synthesis, Ti PTLs were cleaned by using a detergent and a brush under water flow. Afterward, all PTLs were sonicated in ultrapure water until no foaming was observed on top of the water layer. The PTLs were dried under air.

The synthesis of Co_3O_4 on the cleaned Ti PTLs was adapted from the work of Chen et al. [29], Scheme S1. First, varied amounts (3 mmol for the loading of ca. 13.0 ± 0.3 mg cm^{-2} of Co_3O_4 on Ti) of $Co(NO_3)_2 \cdot 6H_2O$ were dissolved in 35 cm^3 (for the higher loadings) or 17.5 cm^3 (for the lower loadings) of H_2O. Then, 8 mmol of NH_4F and 14 mmol of $CO(NH_2)_2$ were added to the solution and stirred until complete dissolution. Afterwards, the Ti PTL was placed at the bottom of the 100 cm^3 Teflon-lined autoclave, where subsequently the prepared solution was added. It was then heated up to 120 °C for 12 hours. After cooling to room temperature, the Ti PTL covered with the Co precursor was removed from the autoclave, cleaned with water, dried, and transferred to the crucible for calcination at 400 °C for 1 hour in air atmosphere in a muffle furnace. The heating rate was set to 1 °C min^{-1} to avoid rapid heating and thus destruction of the formed oxide layers. The final loading of Co_3O_4 on the Ti PTLs was obtained gravimetrically.

Control measurements were performed using Ir black as the anode catalyst. 150 mg catalyst was dispersed in 1:1 ultrapure water:IPA (7.5 cm^3 total volume). 15 wt% PiperION was added to the catalyst dispersion, which was homogenized for 20 min in an ultrasonic bath. The dispersion was spray-coated on the Ti PTL using an airbrush and compressed air. The catalyst loading was maintained at 1 mg cm^{-2} with respect to the metal content. As for the cathode catalyst ink, 196 mg Ag NPs were dispersed in 1:1 ultrapure water:IPA (8 cm^3 total volume). Prior to adding the ionomer (PiperION, 0.3 wt%) the dispersion was homogenized with an immersion sonotrode (Hielscher UP200ST). After adding the ionomer, the dispersion was sonicated further for 20 min in an ultrasonic bath. The dispersion was spray-coated on a Freudenberg H23C6 GDL until reaching 1 mg cm^{-2} metal loading.

Structural and morphological characterization

Crystal structure of the pristine and the used Co_3O_4 layers was determined by X-ray diffraction (XRD) using a Rigaku MiniFlex II instrument equipped with a Cu Kα (λ = 1.5418 Å) X-ray source. Operating conditions were 30 kV, 15 mA in the 5°–80° 2Θ range, with a scan speed of 1.0° min^{-1}.

The composition and morphology of the anode catalyst layer were scrutinized with scanning electron microscopy (SEM, Thermo Scientific Apreo 2) equipped with an energy-dispersive X-ray detector.

X-ray photoelectron spectroscopy (XPS, Al Kα $h\nu$ = 1486.6 eV) was used to reveal the surface composition of the anode catalyst layers. XPS was employed with a SPECS instrument equipped with a PHOIBOS 150 MCD 9 hemispherical analyzer. It was used in a fixed analyzer transmission mode with 40 eV pass energy for the survey scans and 20 eV pass energy for the high-resolution scans. Charge referencing was done to the adventitious carbon (284.8 eV) on the surface of the sample. Spectra were evaluated using the CasaXPS software package.

Electrolysis experiments

All electrochemical results presented in this study were performed in a custom-designed zero-gap electrolyzer cell (A = 8 cm^2). Details on the structure of the cell and further information are available in our precedent publications[3,30,31]. The Co_3O_4-modified Ti PTLs were employed as the anode of the cell, while the Ag NPs-coated Freudenberg H23C6 GDE was used as the cathode in all cases. The anode and cathode compartments were separated with a 40 µm thick PiperION AEM, which was activated and stored in 1.0 M CsOH at least 24 h prior to use. Humidified CO_2 or Ar (in the case of the water electrolysis control experiments) was fed to the cathode with a flow rate of 100 cm^3 min^{-1}, while a 0.05 M CsOH solution was used as the anolyte, which was saturated with CO_2 prior to the electrolysis measurements (to yield $CsHCO_3$) and pumped to the anode compartment of the cell with a flow rate of ca. 70 cm^3 min^{-1}. 100 cm^3 electrolyte was recirculated over the course of the measurements. The gas flow rate was controlled by a Bronkhorst MASS-STREAM D-6321 type mass flow controller. The cell temperature was maintained at 60 °C throughout the measurements.

All electrochemical measurements were performed using a BioLogic VMP-300 potentiostat/galvanostat equipped with an impedance module and a 5 A/10 V booster. The reported current density values correspond to normalizing the current measured by the geometric active area of the cell. The electrochemical protocol consisted of recording three linear sweep voltammograms (LSVs) in the potential range of 0.8 V and 3.2 V (Ir black anode) or 3.4 V (Co_3O_4 anode). This was followed by 30-minute-long potentiostatic experiments at different fixed cell voltages of 2.8 – 3.4 V, ΔU = 0.2 V. The protocol was finished by recording an electrochemical impedance spectrum at the cell voltage value that was applied in the given potentiostatic experiment. The formed CO2RR products were quantified with either a Shimadzu Nexis-GC-2030 gas chromatograph, equipped with a barrier discharge ionization detector or with an online infrared-thermal conductivity gas analyzer (Gasboard-3100, customized for CO_2-CO-H_2 mixtures, Hubei Cubic-Ruiyi). The latter allowed the quantification of gas phase products in real-time. Long-term measurements were performed using the same test framework described above. For evaluating the long-term stability of the catalyst layer, a galvanostatic protocol was used by applying 250 mA cm^{-2} current density. The current density was ramped up in two steps to this value by applying 100 mA cm^{-2} and 200 mA cm^{-2} current density, each for an hour, prior to reaching the 250 mA cm^{-2} value.

Ex-situ ICP-MS measurements

The electrolytes collected after the cell operation were analyzed by inductively-coupled plasma mass spectrometry (ICP-MS, PerkinElmer NexION 350X). ICP-MS was calibrated prior to each set of measurements by a four-point calibration slope (0, 0.5, 1.0, and 5.0 μg L^{-1}) prepared from standard solutions that contained ^{59}Co and ^{48}Ti in each concentration. ^{74}Ge and ^{45}Sc were used as an internal standards for Co and Ti, respectively. The internal standard solution was prepared in 1% HNO_3 electrolyte and was introduced to the nebulizer of the ICP-MS via a Y-connector. All the analyzed electrolytes were diluted 100 times, and this dilution factor was considered when calculating the concentrations of the dissolved species.

Results and Discussion

We employed a straightforward two-step synthesis route adapted from the literature[29] to grow the cobalt oxide layers on the Ti mesh. Scheme S1 demonstrates the concept and the synthesis steps, which include (1) mixing the cobalt nitrate as a precursor and two surfactants (or growth-directing agents)[32,33]: urea and ammonium fluoride (NH_4F), in water; (2) performing a hydrothermal step overnight; and (3) calcining the obtained materials at 400 °C on air. By changing the concentration of the precursor, we managed to vary the final loading of Co_3O_4 on the Ti PTL from ca. 2.5 mg cm^{-2} to ca. 13.3 mg cm^{-2}.

The morphology of the synthesized Co_3O_4 electrodes was studied with SEM. As shown in Fig. 1A, Co_3O_4 was deposited with a porous morphology, and coated the surface of the Ti PTL evenly. Co_3O_4 appears as relatively large (several μm in diameter) 2D flakes (Fig. S1), in line with the precedent literature[29]. The homogeneous coating was further confirmed by SEM-EDX maps (Fig. S1 and Table S1). The amount of Co in the sample was 47.9 ± 1.99 at% while the O content was 51.2 ± 2.01at%. The small Ti signal originates from the underlying porous Ti PTL.

The crystal structure and composition of the as-synthesized samples were scrutinized by XRD (Fig. 1B). A total of seven diffraction peaks ((111), (220), (311), (222), (400), (511), (440)) can be identified on the diffractogram recorded for the Co_3O_4 electrode, that match well with the ones detected for the commercial sample and with previous reports in the literature[34–36]. According to these, the synthesized Co_3O_4 bears a face-centered-cubic crystal structure typical for spinels. XRD data was processed further by performing Rietveld refinement (Figs. S2, Fd-3m point group Co_3O_4, a = 8.05671 Å). Based on the analysis, the average crystal domain size is 19 nm, which is identical to the value determined from the Scherrer equation.

The surface composition of Co_3O_4 was analyzed with XPS, where Co, O, and C could only be identified on the survey scans (Figure S3). The adventitious carbon on the sample surface was used for charge referencing (Figure S4). High-resolution scans of the Co $2p_{3/2}$ region (Fig. 1C) suggest that Co_3O_4 is the dominant phase in the case of all samples[37]. Two cobalt chemical environments were considered (octahedrally (Peak 1) and tetrahedrally (Peak 2) coordinated) with their respective satellite features hallmark of spinel structured Co_3O_4. The core-level O1s spectrum (Fig. 1D) was fitted with three peaks corresponding to lattice oxide (33 at%) to surface carbonate/hydroxide (63 at%), and a small amount of adsorbed water (3 at%) at the surface of the sample. The exact components and binding energies used for the fittings are summarized in Table S2.

Figure 2A shows linear sweep voltammograms (LSVs) recorded using either Ir black or Co_3O_4 as the anode catalyst, under identical experimental conditions. In the case of Ir, the current density monotonously increased to reach 600 mA cm^{-2}, after the onset (a cell voltage of 1.85 V is required for Ir to reach 10 mA cm^{-2} current density). Contrastingly, the highest current density that was measured for the Co_3O_4 sample (≈7 mg cm^{-2} loading) was 225 mA cm^{-2} at 3.20 V cell voltage, which is a notable difference between the two systems (in the case of Ir, 100 mA cm^{-2} current density was reached at $U_{cell} = 2.40$ V, while the cell required $U_{cell} = 2.88$ V to achieve the same value for Co_3O_4). The other difference is that in the case of the Co_3O_4 sample, two small peaks appeared at 1.27 V and 1.67 V cell voltage. The first corresponds to the transformation of Co_3O_4 to CoOOH (Co^{2+} to Co^{3+}), while the second appeared due to the further oxidation of the Co^{3+} to Co^{4+} sites (CoO_2 formation)[34,38]. These intermediates play a key role in driving the OER, hence, it starts only after the oxidation of the catalyst surface[38]. The onset of OER is approximately 300 mV more positive compared to what was observed for Ir.

The potentiodynamic experiments were immediately followed by chronoamperometry measurements at different cell voltages (Fig. 2B). In the case of the Co_3O_4 sample, 65 mA cm^{-2} current density was measured at 2.80 V cell voltage. The current rapidly increased with the applied cell voltage reaching almost 315 mA cm^{-2} at 3.40 V. After setting the given cell voltage, the current stabilizes (in the first five minutes) and remains constant throughout the measurement. Contrastingly, around 350 mA cm^{-2} total current was measured at the lowest cell voltage (U_{cell} = 2.80 V) when the Ir black catalyst was the anode, which rose up to almost 450 mA cm^{-2} at 3.20 V. Stabilization of the measured current took notably longer compared to the Co_3O_4-case. CO2RR selectivity is similar regardless of the anode catalyst (Fig. 2C); 85–92% of the passed charge was consumed by CO formation.

After the first CO_2 electrolysis measurements, a control experiment was performed using the same anode (Co_3O_4 and Ir black) and cathode (Ag NPs) catalysts but running

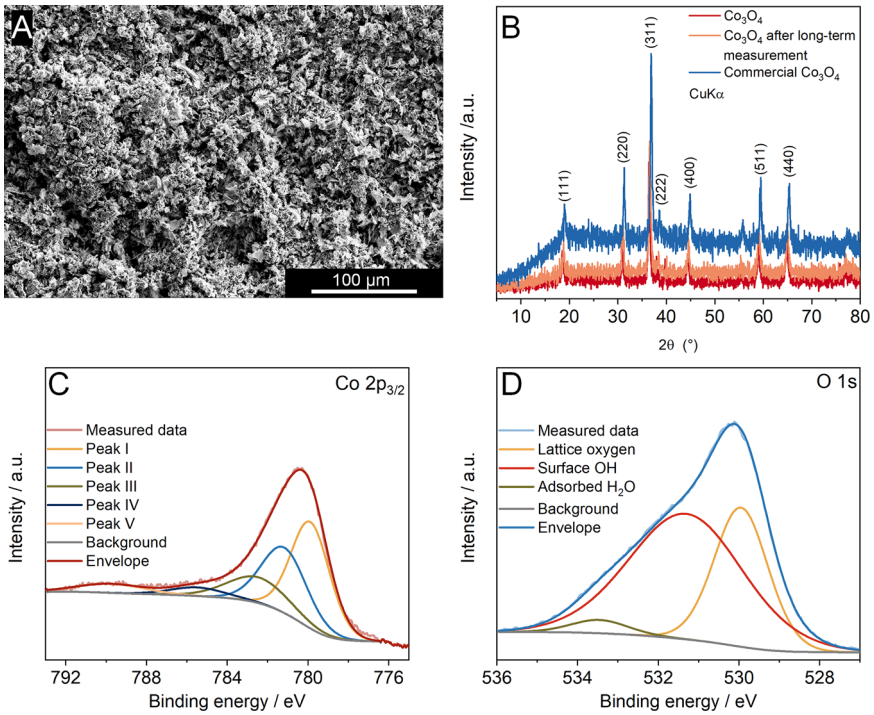

Fig. 1 Physical and morphological characterization of the obtained Co_3O_4 samples. A SEM image recorded for the synthesized Co_3O_4 sample. **B** XRD patterns collected for the as-synthesized Co_3O_4 sample, a Co_3O_4 sample after performing the electrochemical protocol described in the experimental, and for a Co_3O_4 sample acquired from a commercial source. **C**, **D** High-resolution XPS spectra recorded for the Co_3O_4 sample. The catalyst loading on the Ti PTL was ≈ 7 mg cm^{-2}.

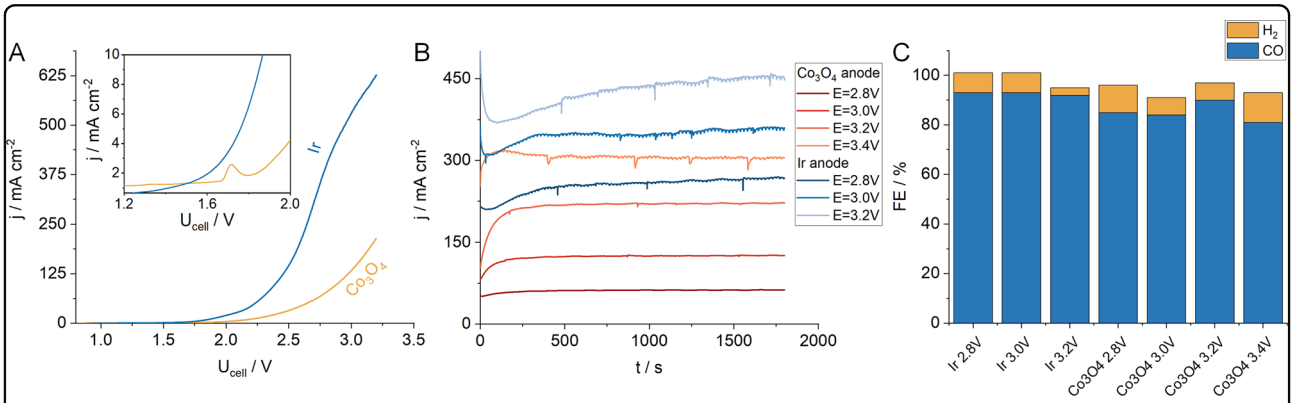

Fig. 2 Electrochemical behavior and CO_2 reduction selectivity. A LSVs recorded for the zero-gap cell employing either Ir or Co_3O_4 as the anode catalyst in 60°C, 0.05 M CsOH electrolyte saturated with CO_2. The sweep rate was 100 mV s^{-1}. Electrolyte and CO_2 flow rates were maintained at 70 cm^3 min^{-1} and 100 cm^3 min^{-1}, respectively. The anode catalyst loading was 1 mg cm^{-2} and 7 mg cm^{-2} for the Ir and Co_3O_4 catalysts, respectively. **B** Chronoamperometry measurements performed at different fixed cell voltages in the range of 2.8 V and 3.4 V for 30 min. Conditions were identical as in the case of (**A**). **C** CO2RR selectivity monitored during the chronoamperometry measurements. Selectivity was determined after the measured current reached a stable value.

water electrolysis instead. The electrolyte was saturated with CO_2 prior to the measurements, but CO_2 was switched to Ar at the start of the electrolysis (Fig. S5). Galvanostatic experiments were performed to facilitate comparison with Ir (i.e., at identical reaction rates). In the case of Co_3O_4, the cell voltage gradually increases with the current density (around 3.05 V at 300 mA cm^{-2}). These values are considerably higher than what is expected from a water electrolyzer cell running with pure water as the electrolyte[22], but the cell voltage remained stable

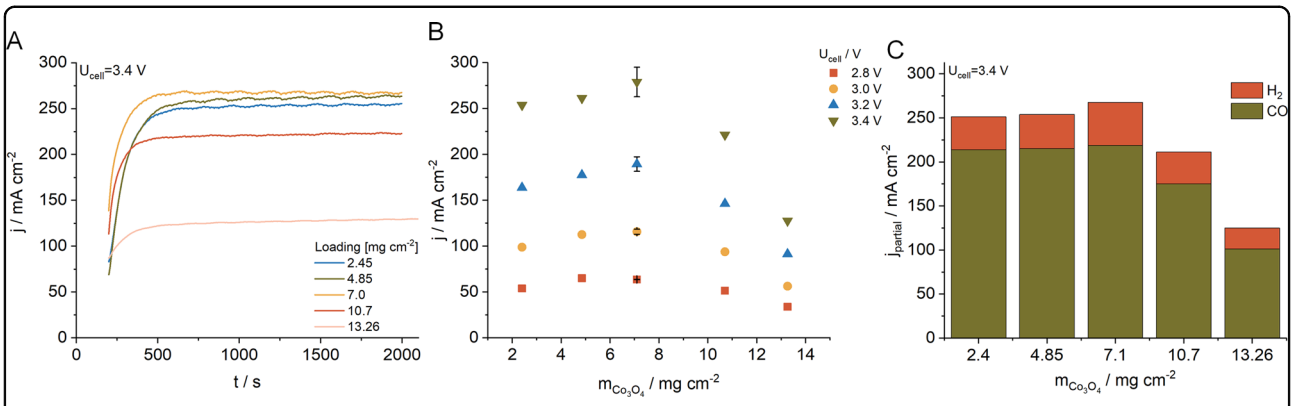

Fig. 3 Loading-dependent electrocatalytic behavior. A Chronoamperometry measurements performed at U_{cell} = 3.40 V varying the loading of the Co_3O_4 anode catalyst in 60°C, 0.05 M CsOH electrolyte saturated with CO_2. Anolyte and CO_2 flow rates were maintained at 70 and 100 cm^3 min^{-1}, respectively. **B** CO2RR selectivity monitored during the chronoamperometry measurements. Selectivity was determined after the measured current reached a stable value. Error bars were calculated from at least two separate measurements, using fresh MEA each time.

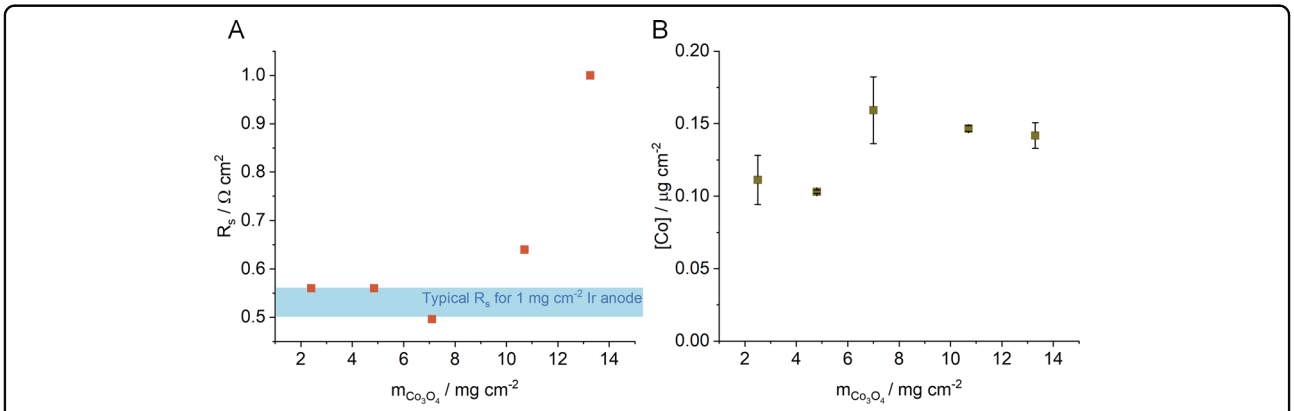

Fig. 4 Electrochemical impedance spectroscopy and ex-situ inductively-coupled plasma mass spectrometry data. A Series resistance values extracted from potentiostatic impedance spectra recorded applying 3.4 V cell voltage and varying the loading of the anode catalyst. Measurements were performed in 60°C, 0.05 M CsOH electrolyte saturated with CO_2 applying 70 cm^3 min^{-1} anolyte, and 100 cm^3 min^{-1} CO_2 flow rate. The blue-shaded area represents a range of R_s values typically determined when Ir is used as the anode catalyst. **B** Dissolved amount of Co determined with ICP-MS from the electrolyte after performing the electrochemical protocol described in the experimental section.

throughout the experiments. When the same measurement was performed with Ir black as the anode, the cell voltage was notably lower (as expected from the previous CO2RR experiments), around 2.57 V at 300 mA cm^{-2} applied current density. Cell voltage remained stable at all three current density values. These values are also higher than the ones typically measured for IrO_2 in water electrolyzer cells (e.g., around 2 V in pure water at 500 mA cm^{-2} current density[22]), most likely because Ag was applied as a HER catalyst and because of the near-neutral pH carbonate buffer electrolyte.

The Co_3O_4 catalyst loading was varied between 2.45 and 13.26 mg cm^{-2}. The achievable current density is visibly affected by the thickness of the catalyst layer (Fig. 3A). The thinner Co_3O_4 layers yield higher current densities than their thicker counterparts, indirectly suggesting that the conductivity of the catalyst layer could be one of the key factors limiting the apparent activity. Besides conductivity, the lower measured current density could be the result of mass-transport limitations developed due to the considerably thicker catalyst layer (especially an issue with higher loadings of 10.7 and 13.26 mg cm^{-2}). The highest current densities at all applied cell voltages were found for the anode catalyst layer with 7.0 mg cm^{-2} loading (for specific values cf. Figure 3B). The measured current density rapidly decreases when the catalyst loading exceeds the optimum value. Figure 3C depicts the CO2RR selectivity data for all the tested Co_3O_4 loadings at 3.40 V applied cell voltage. The CO_2:H_2 ratio is unaffected by the loading of the anode catalyst regardless of the applied cell voltage (see Fig. S6-S10).

To characterize the performance loss experienced for the thicker catalyst layers further, an impedance spectrum was recorded at each applied cell voltage. This was followed by the extraction of the R_s values (Fig. 4A), which

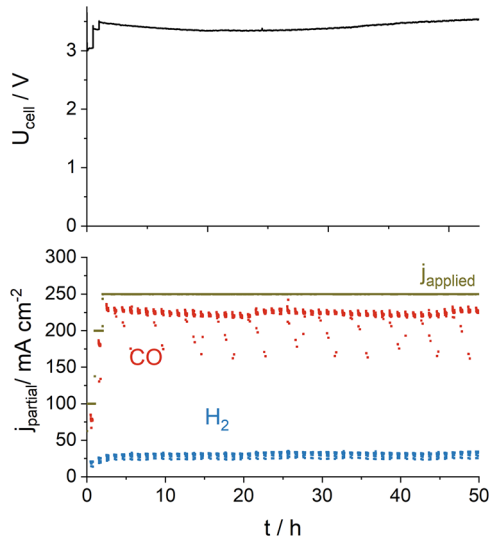

Fig. 5 Long-term CO_2 electrolysis. Long-term chronopotentiometry measurement was performed by applying $j_{total} = 250$ mA cm^{-2} current using a Co_3O_4 anode catalyst with a loading of 4.85 mg cm^{-2}. Data was collected in 60°C, 0.05 M CsOH electrolyte saturated with CO_2. Electrolyte and CO_2 flow rate was maintained at 70 and 100 cm^3 min^{-1}, respectively. CO_2RR selectivity data is presented at the bottom.

are more or less constant until reaching the 7 mg cm^{-2} catalyst loading, but then rapidly increase with the amount of the catalyst deposited on the Ti PTL. The R_s values determined for the Co_3O_4 samples with low-loading (until 7 mg cm^{-2}) are similar to the values typically experienced when Ir black is used as the anode catalyst.

The amount of Co_3O_4 dissolved/detached during electrolysis was quantified by ex-situ ICP-MS measurements (Fig. 4B). The as-prepared Co_3O_4 catalyst layers were rather porous, which might lead to the detachment of at least part of the catalyst layer due to the moderate electrolyte flow rate. ICP-MS data can provide information only on the amount of Co dissolved during electrolysis; it is not able to directly quantify the amount of potentially detached Co_3O_4 nanoparticles. At low Co_3O_4 loadings, the Co loss due to dissolution is around 0.1 µg cm^{-2} (e.g., it is around $2{\cdot}10^{-3}$ w% in the case of the sample with 4.85 mg cm^{-2} loading), while this value increases above 0.158 µg cm^{-2} when the oxide loading reaches 7 mg cm^{-2}. All in all, the amount of dissolved Co seemingly does not change notably by the increasing catalyst loading. Based on these dissolved Co amounts, it can be concluded that the synthesized Co_3O_4 nanosheet anode catalysts are reasonably stable under conditions that develop in zero-gap CO_2 electrolyzer cells (carbonate electrolyte and high carbonate flux through the AEM, near-neutral pH).

To assess the long-term stability of the CO_2 electrolyzer cell equipped with the Co_3O_4 anode catalyst layer, long-term chronopotentiometry experiments were conducted using an in-house developed automated test station[39]. First, tests were performed employing the anodes with 7 mg cm^{-2} catalyst loading, applying 300 mA cm^{-2} constant current density (Figure S11). The cell voltage and the CO2RR selectivity remained stable for the first 20 hours of the 50 hours of constant operation, and then the CO selectivity decreased gradually. This was followed by the disassembly of the electrolyzer cell and the MEA. A series of small pinholes were observed in the membrane that probably formed upon cell assembly and increased in size slowly during operation. It might be that the morphology of the Co_3O_4 nanosheets (sharp edges) caused this issue (see images captured at higher magnification in Fig. S1). To test this hypothesis, an anode Co_3O_4 layer with 4.85 mg cm^{-2} catalyst loading was used (i.e., an anode having a less rough surface). The applied final current density was also decreased to 250 mA cm^{-2}, and it was ramped up in a series of 100, 200 mA cm^{-2}, each one was held for an hour prior to reaching the final value (Fig. 5). Cell voltage was stable over the course of the measurement revolving around 3.40–3.50 V. CO2RR selectivity remained constant for 50 hours with around 90% FE towards CO formation. The anolyte pH was monitored throughout the measurement. The measured pH values were scattered in between 7.05 and 7.30 meaning that the electrolyte preserved its near-neutral character over the course of the experiment under which Co_3O_4 is stable.

After the successful long-term experiment, the cell was disassembled, and the MEA components were scrutinized. Figure S12 shows the SEM images recorded after the measurement. The original plate-like structures transformed to needle-like features on the top of the catalyst layer. EDX analysis (Table S1) shows a decrease in the amount of Co, along with an increase in the O-content and in the recorded Ti signal. The latter suggests that at least part of the catalyst layer either detached from the surface to the electrolyte or stuck to the AEM upon disassembly, decreasing the catalyst layer thickness, which can be penetrated by the electrons reaching even the underlying Ti paper PTL. High-resolution Co $2p_{3/2}$ XPS spectra (Figure S13) suggest the formation of CoOOH phase besides Co_3O_4, which is in line with the experienced morphology change. The O1s peak shifted towards lower binding energies after the measurement, implying also the formation of the oxohydroxide phase (lattice oxide is around 45 at%, while the surface hydroxide is around 55 at%). Contrastingly, XRD of the as-synthesized Co_3O_4 (Fig. 1C) and the one after the long-term experiment are identical, indirectly indicating that the previously described alterations appeared only at the catalyst surfac,e leaving the bulk unchanged. No Co was detected within or on the cathode side of the AEM by looking at the EDX mapping data (Figure S14). The membrane remained intact throughout the measurement;

using the lower Co_3O_4 loading, no holes can be observed by the naked eye in the membrane.

Conclusions

In this proof-of-concept study, Ir was replaced by porous Co_3O_4 nanosheets and employed as an anode catalyst in a CO_2 electrolyzer cell. To alleviate conductivity issues intrinsically originating from the semiconducting nature of Co_3O_4 and from the inadequate connection between the PTL and the catalyst particles, Co_3O_4 was directly synthesized on the surface of the Ti paper PTL by a simple hydrothermal method. This approach allowed the precise tailoring of the catalyst loading. 7 mg cm^{-2} catalyst loading was found to be optimal, the measured current densities reached around 300 mA cm^{-2} at 3.4 V applied cell voltage. Additionally, only a marginal amount of Co leached to the electrolyte during the several hours-long electrochemical protocol. The CO_2 electrolyzer with Co_3O_4 as the anode catalyst was operated galvanostatically continuously for over 50 hours, applying 250 mA cm^{-2} current density. CO2RR selectivity and U_{cell} remained stable throughout the measurement. Our results indicate that Co_3O_4 can withstand the conditions developing during long-term CO_2 electrolysis (near-neutral pH, carbonate-containing electrolyte). The presented results could be further improved by optimizing the initial morphology of Co_3O_4 or by introducing other metals in the spinel crystal structure (therefore improving the conductivity of the oxide requiring the deposition of less material on the Ti PTL). Overall, we demonstrated that it is possible to replace Ir with more abundant, non-noble, and, hence, financially more favorable alternatives. The presented synthesis method is readily scalable; only the size of the hydrothermal reactor is the limit. These together can support the penetration of CO_2 electrolysis technology at an industrial level.

Acknowledgements

Project no. RRF-2.3.1-21-2022-00009, titled National Laboratory for Renewable Energy has been implemented with the support provided by the Recovery and Resilience Facility of the European Union within the framework of Programme Széchenyi Plan Plus. T.P. acknowledges the financial support of the Alexander von Humboldt Foundation. eChemicles Zrt acknowledges funding from the Hungarian NRDI Fund, through the 2021-1.1.4-GYORSÍTÓSÁV-2022-00029 project.

Author details

[1]Department of Physical Chemistry and Materials Science, University of Szeged, Rerrich Square 1, Szeged, Hungary. [2]Forschungszentrum Jülich GmbH, Helmholtz-Institute Erlangen-Nürnberg for Renewable Energy (IET-2), Cauerstraße 1, Erlangen, Germany. [3]Department of Molecular and Analytical Chemistry, University of Szeged, Dóm Square 7-8, Szeged, Hungary. [4]Interdisciplinary Excellence Center, University of Szeged, Rerrich Square 1, Szeged, Hungary. [5]eChemicles Zrt, Alsó Kikötő sor 11, Szeged, Hungary

Author contributions

C.J., S.C., T. P., E.B. and A.K conceived the idea and designed the research. T.P. synthesized the catalyst samples used in this study. A.K. performed all the electrochemical measurements and analyzed the collected data. G.F.S. gathered and analyzed the XPS data. A. S. performed the SEM-EDX measurements. A. K. wrote the first version of the manuscript. All authors contributed to interpreting the results and revising the manuscript.

Funding

Open access funding provided by University of Szeged.

Competing interests

eChemicles is developing and commercializing CO_2 electrolyzer systems.

Ethics

No humans or living organisms were subject of the study. In terms of research practices, all methods were performed in accordance with the relevant guidelines and regulations.

Supplementary information The online version contains supplementary material available at https://doi.org/10.1038/s41427-025-00598-4.

Received: 19 November 2024 Accepted: 20 March 2025.
Published online: 25 April 2025

References

1. Vass, A., Kormányos, A., Kószó, Z., Endrődi, B. & Janáky, C. Anode catalysts in CO2 electrolysis: challenges and untapped opportunities. *ACS Catal.* **12**, 1037–1051 (2022).
2. Xu, Q. et al. Identifying and alleviating the durability challenges in membrane-electrode-assembly devices for high-rate CO electrolysis. *Nat. Catal.* **6**, 1042–1051 (2023).
3. Vass, et al. Local chemical environment governs anode processes in CO2 electrolyzers. *ACS Energy Lett.* **6**, 3801–3808 (2021).
4. Li, Q. et al. Anion exchange membrane water electrolysis: the future of green hydrogen. *J. Phys. Chem. C.* **127**, 7901–7912 (2023).
5. Dong, Y., Oloman, C.W., Gyenge, E.L., Su, J. & Chen, L. Transition metal based heterogeneous electrocatalysts for the oxygen evolution reaction at near-neutral pH. *Nanoscale* **12**, 9924–9934 (2020).
6. Jiang, N., Zhu, Z., Xue, W., Xia, B.Y. & You, B. Emerging electrocatalysts for water oxidation under near-neutral CO2 reduction conditions. *Adv. Mater.* **34**, 1–22 (2022).
7. Joya, K.S., Takanabe, K. & de Groot, H.J.M. Surface generation of a Cobalt-derived water oxidation electrocatalyst developed in a neutral HCO3−/CO2 System. *Adv. Energy Mater.* **4**, 2–7 (2014).
8. Meng, Y. et al. Highly active oxygen evolution integrated with efficient CO2 to CO electroreduction. *Proc. Natl Acad. Sci.* **116**, 23915–23922 (2019).
9. Joya, K.S., Joya, Y.F. & de Groot, H.J.M. Ni-based electrocatalyst for water oxidation developed in-situ in a HCO3− /CO2 system at near-neutral pH. *Adv. Energy Mater.* **4**, 3–7 (2014).
10. Chen, Z., Kang, P., Zhang, M.-T., Stoner, B.R. & Meyer, T.J. Cu(ii)/Cu(0) electrocatalyzed CO2 and H2O splitting. *Energy Environ. Sci.* **6**, 813 (2013).
11. Chen, Z. & Meyer, T.J. Copper(II) Catalysis of water oxidation. *Angew. Chem. Int. Ed.* **52**, 700–703 (2013).
12. Marcel Pourbaix. *Atlas of Electrochemical Equilibria in Aqueous Solutions*. (National Association of Corrosion Engineers, 1974).
13. Kanan, M.W., Surendranath, Y. & Nocera, D.G. Cobalt–phosphate oxygen-evolving compound. *Chem. Soc. Rev.* **38**, 109–114 (2009).
14. Burke, L.D., Lyons, M.E. & Murphy, O.J. Formation of hydrous oxide films on cobalt under potential cycling conditions. *J. Electroanal. Chem. Interfacial Electrochem.* **132**, 247–261 (1982).
15. Yu, M., Budiyanto, E. & Tüysüz, H. Principles of water electrolysis and recent progress in Cobalt-, Nickel-, and Iron-based oxides for the oxygen evolution reaction. *Angew. Chem. Int. Ed.* **61**, e202103824 (2022).
16. Zhang, W., Cui, L. & Liu, J. Recent advances in cobalt-based electrocatalysts for hydrogen and oxygen evolution reactions. *J. Alloy. Compd.* **821**, 153542 (2020).

17. Bergmann, A. et al. Reversible amorphization and the catalytically active state of crystalline Co3O4 during oxygen evolution. *Nat. Commun.* **6**, 8625 (2015).
18. Wang, C., Deng, R., Guo, M. & Zhang, Q. Recent progress of advanced Co3O4-based materials for electrocatalytic oxygen evolution reaction in acid: from rational screening to efficient design. *Int. J. Hydrog. Energy* **48**, 31920–31942 (2023).
19. Cherevko, S. Stabilization of non-noble metal electrocatalysts for acidic oxygen evolution reaction. *Curr. Opin. Electrochem.* **38**, 101213 (2023).
20. Mondschein, J.S. et al. Crystalline Cobalt oxide films for sustained electrocatalytic oxygen evolution under strongly acidic conditions. *Chem. Mater.* **29**, 950–957 (2017).
21. Natarajan, K., Munirathinam, E. & Yang, T.C.K. Operando investigation of structural and chemical origin of Co3O4stability in acid under oxygen evolution reaction. *ACS Appl. Mater. Interfaces* **13**, 27140–27148 (2021).
22. Krivina, R.A. et al. Anode catalysts in anion-exchange-membrane electrolysis without supporting electrolyte: conductivity, dynamics, and ionomer degradation. *Adv. Mater.* **34**, 1–10 (2022).
23. Zhang, L., Xu, Q., Hu, Y., Chen, L. & Jiang, H. Benchmarking the pH–stability relationship of metal oxide anodes in anion exchange membrane water electrolysis. *ACS Sustain. Chem. Eng.* **11**, 13251–13259 (2023).
24. Wang, N. et al. Strong-Proton-adsorption co-based electrocatalysts achieve active and stable neutral seawater splitting. *Adv. Mater.* **35**, 1–7 (2023).
25. Yan, Q. et al. Chromium-induced high covalent Co–O bonds for efficient anodic catalysts in PEM electrolyzer. *Adv. Sci.* **11**, 1–8 (2024).
26. Wang, Y. et al. Tuning the Co pre-oxidation process of Co3O4 via geometrically reconstructed F–Co–O active sites for boosting acidic water oxidation. *Energy Environ. Sci.* https://doi.org/10.1039/D4EE03982C (2024).
27. Yu, P.C. et al. Nitrogen-mediated promotion of cobalt-based oxygen evolution catalyst for practical anion-exchange membrane electrolysis. *J. Am. Chem. Soc.* **146**, 20379–20390 (2024).
28. Faisal, F. et al. Atomically defined Co3O4 (111) thin films prepared in ultrahigh vacuum: stability under electrochemical conditions. *J. Phys. Chem. C.* **122**, 7236–7248 (2018).
29. Chen, G.-Y. et al. Engineering cationic vacancies in octahedral sites of Co3O4 for high-efficiency oxygen evolution. *Energy Fuels* **37**, 8523–8530 (2023).
30. Samu, A.A., Szenti, I., Kukovecz, A., Endrődi, B. & Janáky, C. Systematic screening of gas diffusion layers for high performance CO2 electrolysis. *Commun. Chem.* **6**, 41 (2023).
31. Endrődi, B. et al. High carbonate ion conductance of a robust PiperION membrane allows industrial current density and conversion in a zero-gap carbon dioxide electrolyzer cell. *Energy Environ. Sci.* **13**, 4098–4105 (2020).
32. Di, Y. et al. Effect of urea and ammonium fluoride ratio on CuCo2S4 /NF as a highly efficient HER catalyst. *RSC Adv.* **13**, 28713–28728 (2023).
33. Kiaeerad, P. & Naji, L. Synergistic effect of two complexing agents on the hydrothermal synthesis of self-supported ZnNiCo oxide as electrode material in supercapacitors. *J. Electroanal. Chem.* **901**, 115779 (2021).
34. Adhikari, H. et al. Synthesis and electrochemical performance of hydrothermally synthesized Co3O4 nanostructured particles in presence of urea. *J. Alloy. Compd.* **708**, 628–638 (2017).
35. Yetim, N.K. Hydrothermal synthesis of Co3O4 with different morphology: Investigation of magnetic and electrochemical properties. *J. Mol. Struct.* **1226**, 129414 (2021).
36. Diallo, A., Beye, A.C., Doyle, T.B., Park, E. & Maaza, M. Green synthesis of Co3O4 nanoparticles via Aspalathus linearis: Physical properties. *Green. Chem. Lett. Rev.* **8**, 30–36 (2015).
37. Biesinger, M.C. et al. Resolving surface chemical states in XPS analysis of first row transition metals, oxides and hydroxides: Cr, Mn, Fe, Co and. *Ni. Appl. Surf. Sci.* **257**, 2717–2730 (2011).
38. Kang, W. et al. Unraveling sequential oxidation kinetics and determining roles of multi-cobalt active sites on Co3O4 catalyst for water oxidation. *J. Am. Chem. Soc.* **145**, 3470–3477 (2023).
39. Samu, A.A. et al. Intermittent operation of CO2 electrolyzers at industrially relevant current densities. *ACS Energy Lett.* **7**, 1859–1861 (2022).